IEEE Access
Multidisciplinary | Rapid Review | Open Access Journal

Received September 25, 2019, accepted October 22, 2019, date of publication October 29, 2019,
date of current version November 13, 2019.

Digital Object Identifier 10.1109/ACCESS.2019.2950278

Efficient Acquisition Method for Marine Monitoring Data Based on Compressed Sensing

WENBIAO TIAN, (Member, IEEE), GUOSHENG RUI, GE LIU, AND DAOGUANG DONG
Signal and Information Processing Provincial Key Laboratory in Shandong, Naval Aviation University, Yantai 264001, China

Corresponding author: Wenbiao Tian (twbi5si@gmail.com)

This work was supported by the National Natural Science Foundation of China under Grant 41606117, Grant 41476089, and Grant 61671016.

ABSTRACT There is a prominent contradiction between the existing resolution requirements of marine monitoring data (MMD) and the cost of sensor network deployment. This article proposes an MMD acquisition and reconstruction scheme based on compressed sensing theory (CS-MMD). Firstly, the sparse characteristics of the measured MMD are analyzed and modeled as a multi-measurement vector (MMV) compressed sensing reconstruction problem. Furthermore, the operating state of the sensor is adjusted by a random sparse polynomial distribution matrix. The sensors corresponding to the non-zero elements in the matrix work with a probability of p (small value), and the rest of the sensors sleep. In the reconstruction, the energy prior of the data is fully used to obtain the support set, and the MMV is randomly reduced to the SVM to simplify the support set reconstruction process. The theoretical analysis gives the conditions for accurate reconstruction. The simulation results show that CS-MMD can save a lot of acquisition resources and accurately reconstruct data, and the accuracy rate reaches 99% under the premise of saving up to 99% of sampling resources.

INDEX TERMS Compressed sensing, sparse data recovery, multiple measurement vector, orthogonal matching pursuit, marine monitoring data.

I. INTRODUCTION

The ocean is an important base for human survival, reproduction and socially sustainable development. With the substantial increase in the economic, military, and technological strengths of the world and the growing demand for resources, mankind has begun to shift its line of sight from land to a wider ocean. In recent years, countries have paid more and more attention to maritime rights, and the enthusiasm for the development and utilization of the ocean is emerging globally. In this context, the issue of marine environmental monitoring has begun to receive more and more attention. In order to make up for the shortcomings of large-scale monitoring methods such as satellite remote sensing and radar, the use of sensor networks to acquire various marine environmental factors [1]–[4] (such as temperature, salinity, current, etc.) has become a new research hotspot in the field of marine information.

The associate editor coordinating the review of this manuscript and approving it for publication was Ligang He.

A large number of marine sensor nodes in the sensor network [5] are deployed to designated sea areas, collect various environmental elements in the network distribution area, and then transmit the collected data to the monitoring center through various communication means. Due to the vast ocean area, complex underwater level, and varied environment, marine sensor networks have higher requirements in terms of coverage area breadth and depth compared to traditional terrestrial wireless sensor networks. However, high-resolution monitoring of large-scale sea areas through the intensive and regular deployment of a large number of marine sensor nodes is difficult to achieve. On the one hand, the network construction costs are so many due to the large number of nodes. On the other hand, how to efficiently transmit and process data collected by these sensor nodes is also limited by constraints such as node energy consumption and network bandwidth. In practical applications, from the perspective of system implementation complexity, network energy consumption, bandwidth overhead, and economic cost, it is often necessary to use as few nodes as possible

to achieve information collection in a specified area. In the traditional sensor network information acquisition method, there is an intractable contradiction between the number of nodes required to monitor the specified area and the spatial resolution, which becomes a bottleneck restricting the development of the marine sensor network.

Recently, the theory of compressed sensing (CS) provides a new idea for data acquisition in sensor networks. CS theory points out that people can directly collect the really useful sparse information in redundant data without having to go through the process of high-speed sampling (Nyquist sampling) and then mass dropping (compression). After all, we have witnessed the widespread success of lossy compression formats for sound, imagery, etc. Now we know that most of the data we get is ''can be discarded'' and almost no loss. In other words, we can get sparse and useful information in the data at a much lower sampling rate than the traditional mode.

In order to accurately reconstruct the data, the sparsity of the original data is a necessary condition for compressed sensing, and the sparsity of the data directly determines the number of samples required. However, most of the existing literature directly assumes or acts as an axiom that ''most natural phenomena are sparse or compressible'' [6], but the sparseness of MMD is rarely analyzed. In addition, existing compression sensing schemes often assume that the sparseness of the data is known and fixed. Unfortunately, due to the dynamic nature of the environment, this assumption may not be true for real environmental data.

This paper first analyzes the real marine monitoring data (MMD), revealing the hidden sparse nature of the data. Fully using the sparsity, data acquisition and reconstruction scheme based on compressed sensing theory is proposed, named CS-MMD. The sensor can be intermittently operated without changing the existing sensor network layout, thereby reducing the sampling rate to 1%∼1‰ of the traditional mode and reconstructing useful information by using an optimization algorithm. Due to intermittent sampling, our CS-MMD solution greatly reduces the amount of communication and computational costs. Our contributions are summarized as follows:

- We analyzed many real MMD. The results show that the data have the characteristics of sparsity, time stability and sparsity stability.
- Using the data sparsity stability, a time-space three-dimensional compressed sensing scheme is proposed and modeled as an MMV problem. According to the random sparse matrix control sensor operation or dormancy, the spatiotemporal sampling scale is adjusted by controlling the probability of non-zero value, and the accuracy rate reaches 99% under the premise of saving 99% sampling resources.
- In order to meet the requirements of systems with limited traffic, computing power and power consumption, we make full use of the sparse support set prior to the data and propose a minimally simple reconstruction algorithm to greatly reduce the consumption of the entire system.
- Through the simulation of actual data acquisition and reconstruction, it is proved that our CS-MMD scheme can accurately acquire data at a very low cost. Compared with similar algorithms, the time complexity is the lowest while ensuring the reconstruction accuracy.

II. RELATED WORK

Compressed Sensing focuses on how to accurately recover signals with sparse structures in the case of severe undersampling. The solution is based on a probabilistic model, usually with a series of optimization algorithms to achieve signal recovery. In recent years, CS has become one of the research hotspots in the field of signal processing and has achieved success in different application directions. In CS theory, the Multiple Measurement Vector (MMV) problem is to identify multiple columns of unknown signals with the same sparse support, which has attracted the attention of many scholars. Therefore, in supraharmonics measurement [7], typhoon derivation [8], communication signal processing [9], [10], image processing [11], matrix completion [5], angle of arrival estimation and biometrics, many scholars have found and constructed MMV model with shared support set, and achieved better sparse reconstruction effects and anti-noise performances than single measurement vector (SMV) model. Before the establishment of the MMV model, the idea of solving this kind of problem is to convert the data into one or more SMV problems, and then use the corresponding sparse reconstruction algorithm to perform single vector reconstruction and then combine to get the final solution. Although this processing mode can also obtain good reconstruction results, since each SMV needs to perform one reconstruction, a large number of redundant calculations will be generated, which increases the unnecessary computational burden. In order to solve the problem of high computational complexity in solving MMV, Cotter *et al.* [12] first proposed the sparse reconstruction idea based on MMV and applied it to magnetoencephalography imaging processing.

In recent years, many MMV data recovery algorithms have been proposed. These include a variety of minimization optimization algorithms [13] ($\ell_{2,1}$ minimization [14], M-FOCUSS [12], etc.), greedy algorithms [15], [16] (SA-MUSIC [17], CS-MUSIC [18], SOMP [19] and M-OMP [7], [12], [20], etc.) and Bayesian algorithms (such as MSBL and T-MSBL [21]). However, the performance of many algorithms depends on the measurement matrix [22], [23], data dimension and sparsity, statistical distribution of non-zero elements of the signal, measurement noise power and other parameters [24]. But, when the actual data are collected, these parameters are often unknown and time varying. If there is no prior knowledge of these parameters, the performance of the algorithm will be greatly limited. In addition, some algorithms are not optimized for power consumption and traffic limited systems, and the complexity is large, which is difficult to apply to actual data acquisition.

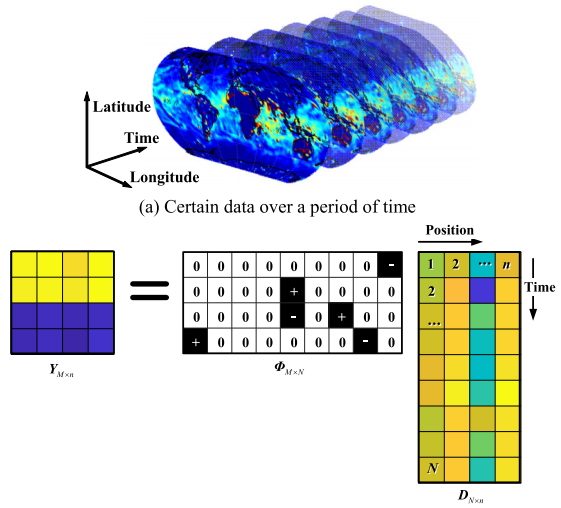

(a) Certain data over a period of time

(b) MMV observation model

FIGURE 1. Schematic diagram of MMV observation of MMD.

III. SPATIO-TEMPORAL SAMPLING MODEL

A. MMV MODEL

The MMV problem solves the joint reconstruction problem of multiple sparse signals with the same support set. Let the sparse signals of the n shared support sets form the signal set $\boldsymbol{X} = \left[\boldsymbol{x}_{:,1}, \boldsymbol{x}_{:,2}, \cdots, \boldsymbol{x}_{:,n}\right] \in \mathbb{R}^{N\times n}$ and the sensing matrix $\boldsymbol{A} \in \mathbb{R}^{M\times N}$. Multiple observation vectors $\boldsymbol{Y} = \left[\boldsymbol{y}_{:,1}, \boldsymbol{y}_{:,2}, \cdots, \boldsymbol{y}_{:,n}\right] \in \mathbb{R}^{M\times n}$ can be expressed as

$$\boldsymbol{Y} = \boldsymbol{A}\boldsymbol{X} \tag{1}$$

where $\boldsymbol{x}_{:,i}$ and $\boldsymbol{y}_{:,i}$ represent the i th ($i = 1, 2, \ldots, n$) column of $\boldsymbol{X}$ and $\boldsymbol{Y}$, respectively, N and M represent the dimension of each signal $\boldsymbol{x}_{:,i}$ and the dimension of each observation vector $\boldsymbol{y}_{:,i}$, respectively.

Any MMV problem can be converted to a standard form of MMV problem by singular value decomposition and dimensionality reduction operations [18].

$$\min_{\boldsymbol{X}} \|\boldsymbol{X}\|_0, \quad \text{s.t. } \boldsymbol{Y} = \boldsymbol{A}\boldsymbol{X} \tag{2}$$

where, $\|\boldsymbol{X}\|_0 = |\text{supp } \boldsymbol{X}| = k$, $\text{supp } \boldsymbol{X} = \left\{1 \le i \le n : \boldsymbol{x}_{i,:} \ne \boldsymbol{0}\right\}$, $\boldsymbol{x}_{i,:}$ is the ith row of $\boldsymbol{X}$.

B. MARINE MONITORING DATA OBSERVATION MODEL

Large-scale buoys at sea, such as the Tropical Atmosphere Ocean project (TAO) and the Argo plan, can collect temperature, pressure, humidity and other data all day. In the natural environment, these data are continuous, slowly varying three-dimensional variables, i.e. sparse (further analysis in Section 4). A novel ocean monitoring data acquisition scheme is proposed, which uses compressed sensing technology for efficient acquisition. Our goal is to effectively schedule the data collection process to significantly reduce the required sensing resources while maintaining acquisition quality.

Fig. 1(a) shows the distribution of a certain data over a period of time. A matrix $\boldsymbol{D}_{N\times n}$ is defined to represent real data within a time measurement window T. In current data acquisition systems, the data sampling interval should at least satisfy Shannon's sampling law. In the data matrix, the columns correspond to the sensed locations and the rows correspond to the moments. Each entry represents monitoring data for a particular location and time. For n sensors randomly distributed in a given area, it is no longer that each sensor collects data periodically and reports it to the receiver. At each time, only some sensors perform sensing and reporting functions according to the requirements of the measurement matrix $\boldsymbol{\Phi}_{M\times N}$ ($\boldsymbol{\Phi}_{M\times N} \cdot \boldsymbol{D}_{N\times n}$). The elements in $\boldsymbol{\Phi}_{M\times N}$ are bounded, independently and identically distributed and the mean zero. Let the column of the measurement matrix have a unit norm in the expectation sense. Let ϕ_{ij} ($i \in [1, M]$, $j \in [1, N]$) be the (i, j) element of $\boldsymbol{\Phi}$, then the distribution of each element is

$$\phi_{ij} \overset{\text{i.i.d}}{\sim} \begin{cases} 1/\sqrt{Mp} & \text{with prob.} p/2 \\ 0 & \text{w.p.} 1-p \\ -1/\sqrt{Mp} & \text{w.p.} p/2 \end{cases}, \quad p \in (0, 1) \tag{3}$$

The probability of a non-zero element is p, expressed by a black block, that is, a data collection point. The probability of 0 is $1 - p$ represented by a white block, that is, a non-acquisition point, as shown in Fig. 1 (b). From a spatial point of view, only part of the data are collected at a certain time. From the time point of view, the data collection at a certain position in the space is not continuous, and only the time corresponding to the black block is collected. If the buoy system is taken as an example, only the buoy corresponding to the black block works and the remaining buoys are in a dormant state. Finally, a $M \times n$ dimensional observation matrix $\boldsymbol{Y}_{M\times n}$ is obtained, where M is the number of observations. Thus, the sampling rate is actually determined by M and p, and the ratio of the method in this paper to the number of samples in the traditional method is actually $r = Mp$.

At this point, the observation of $\boldsymbol{Y}_{M\times n} = \boldsymbol{\Phi}_{M\times N} \cdot \boldsymbol{D}_{N\times n}$ seems to dissatisfy the MMV definition of the (1). Considering the data sparsity that will be further analyzed in Section IV, the data matrix $\boldsymbol{D}_{N\times n}$ is sparse under some transformation, the base is $\boldsymbol{\Psi}_{N\times N}$ and $\boldsymbol{D} = \boldsymbol{\Psi}\boldsymbol{X}$ is satisfied. Where each column of $\boldsymbol{X}$ is equivalent to the sparse coefficient of the column corresponding to the original data, then the observation equation is

$$\boldsymbol{Y} = \boldsymbol{\Phi} \cdot \boldsymbol{D} = \boldsymbol{\Phi} \cdot \boldsymbol{\Psi}\boldsymbol{X} = \boldsymbol{A}\boldsymbol{X} \tag{4}$$

Let $\boldsymbol{A}$ be the new sensing matrix, then (4) is consistent with (1).

Before the Minimalist reconstruction (MR) algorithm is proposed in Section V, we will first analyze a set of measured MMD to better illustrate the sparse characteristics of the data.

IV. MEASURED DATA ANALYSIS

The simulation experiment of CS-MMD high-efficiency acquisition was carried out using the measured data of the Tropical Atmosphere Ocean (TAO) project.

The measured data parameters used are as follows:

Time range: April 01, 2011 - May 01, 2011

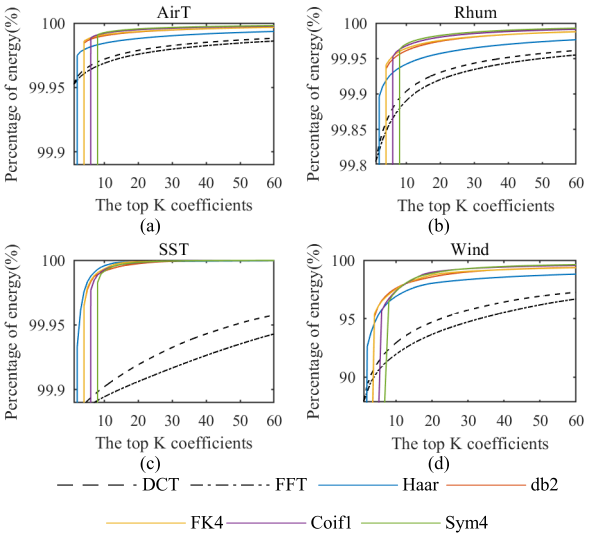

FIGURE 2. Percentage of energy captured by the top K term sparse coefficients.

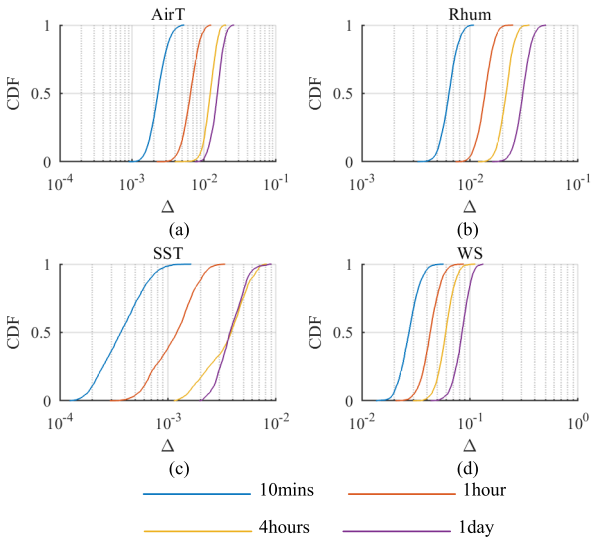

FIGURE 3. Time stability of MMD.

Time resolution: 10 mins
Spatial range: 165°E ∼ 95°W; 8°S ∼ 8°N
Spatial resolution: Irregular (refer to the data website)

TAO / TRITON and PIRATA buoys measure more than 20 kinds of meteorological parameters on the ocean and sea surface. This article is limited to the length of only a few typical data analysis, such as Air temperature (AirT) measured at 3 meters above the sea surface, Relative Humidity (Rhum) measured at 3 meters above the sea surface, Sea surface temperature (SST) measured at 1 meter below the sea surface, the speed of winds (WS) at 4 meters above the sea surface.

A. SPARSITY

Few documents specifically analyze MMD sparsity and discuss under what transform domain they are sparsest. Therefore, three kinds of sparse analysis methods, such as discrete cosine transform (DCT), fast Fourier transform (FFT) and wavelet decomposition (DWT), which are commonly used in signal processing, are introduced to analyze the measured data. Among DWT, five different bases were selected, including Haar, Daubechies-2 (db2), Coiflet-1 (Coif1), Fejér-Korovkin-4 (FK4), and Symlet-4 (Sym4).

The measured data are decomposed on the above sparse basis, and the percentage of energy captured by the top K term sparse coefficients is analyzed. The average results of all sensors are shown in Fig. 2. The abscissa is K, and the ordinate is the percentage of energy captured by the previous K coefficients with the largest amplitude. Note that the raw data time resolution is 10 mins, then each sensor will produce 4464 sample points over the time range of interest. From the overall view of Fig. 2, the top 10 coefficients of the four marine data capture more than 90% of the energy. For AirT, Rhum and SST, the energy captured by the top 10 coefficients even reached more than 99%. This shows that the decomposition coefficients are sparse or compressible, i.e. most energy (>90%) or useful information is concentrated on a very small number (<2.2‰) of coefficients. The sparsity of wavelet decomposition coefficients is generally better than DCT and FFT. For example, under Haar decomposition, the first two coefficients (0.448‰) can capture more than 92% of the data energy, and even capture more than 99.9% for AirT, Rhum and SST. They carry most of the useful information. These results show that the data matrix has good sparsity or compressibility in the studied scene, which lays the foundation for subsequently compressed sensing.

B. TIME STABILITY

MMD typically change over time continually. This section studies the instantaneous stability of MMD by calculating the relative difference between adjacent time data at each location, as defined by (5)

$$\Delta(i,t) = \frac{1}{n}\sum_{j=1}^{n}\frac{\left|d_{i,j} - d_{i-t,j}\right|}{\max\limits_{i,j}\left|d_{i,j}\right|} \tag{5}$$

Among them, $d_{i,j}$ is the element of the ith row and the jth column in $\boldsymbol{D}$, that is, the value acquired by the jth sensor at time i. The numerator $\left|d_{i,j} - d_{i-t,j}\right|$ is the data difference between t sampling intervals. Here, t can be taken 1, 6, 24, 144, that is, the difference of data at 10 minutes, 1 hour, 4 hours and 1 day is compared. All sensors are averaged and the cumulative distribution is statistically as shown in Fig. 3.

It can be seen from Fig. 3 that the relative change of the MMD over time is less than 10%, especially when the time interval is short (such as 10 minutes), the probability that the SST relative change is less than 10^{-3} is greater than 98%. The wind speed varies greatly with respect to the other three quantities, but the probability of a change of less than 3% in 10 minutes is greater than 90%. This shows the time stability of real data and partly explains why the MMD are sparse or compressible.

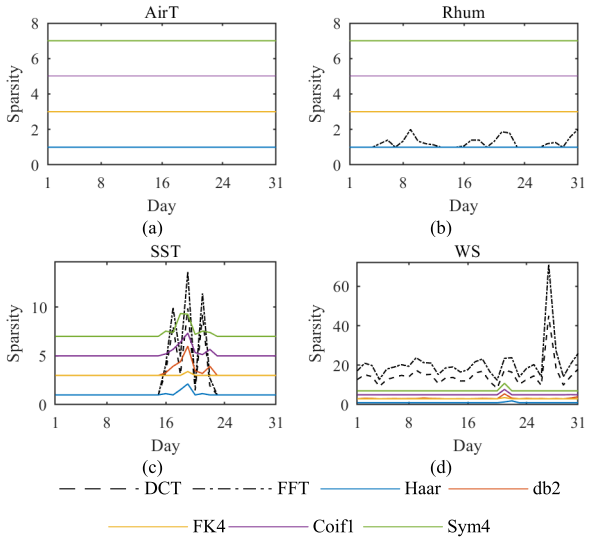

FIGURE 4. Sparse stability of MMD.

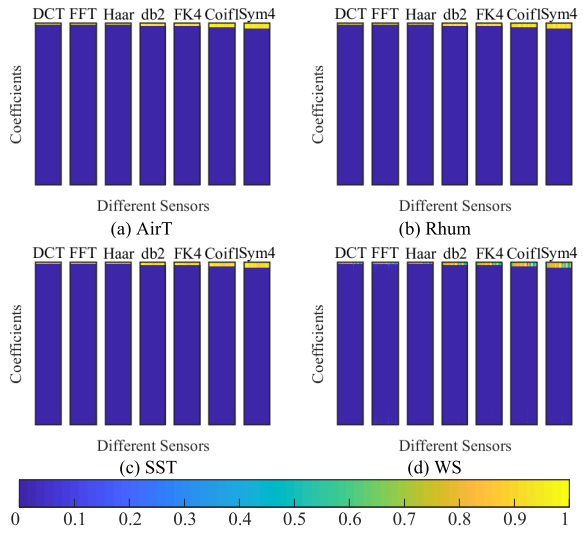

FIGURE 5. Spatial similarity of MMD.

C. SPARSE STABILITY

It is known from the above analysis that MMD are sparse.

Definition 1 (Energy Sparsity): If the largest pre-K term coefficients of the sparseness coefficients $\boldsymbol{x}_{:,i}$ occupies more than $q\%$ of the total energy, the $q\%$-energy sparsity of $\boldsymbol{x}_{:,i}$ is K.

The energy sparsity of the data is actually different from the signal sparsity in the previous literature. For general signals, the sparsity is often unknown and time-varying, while the energy sparsity can be estimated based on the signal model. For example, Candes and Tao [25] model the sparse coefficients of data as exponential decay, satisfying

$$|x|_{(n)} \leq R \cdot n^{-1/s}, \quad R,\ s > 0 \tag{6}$$

where $|x|_{(n)}$ represents the nth of the sparse coefficients $\boldsymbol{x}_{:,i}$ amplitude arranged from largest to smallest. Thus, once our sparse basis is selected, the K value can be estimated based on the definition of energy sparsity.

Taking 24 hours as the width of the time window, sliding the window in steps of 100 minutes, analyzing the daily energy sparsity of the MMD, and synthetically investigating the sparsity stability. It is known from the previous chapters that the sparsity of AirT, Rhum, and SST is better than wind speed (coefficient energy is more concentrated), so the 99.9% energy sparsity is investigated, and q is taken as 99 for the wind speed. The result is shown in Fig. 4.

As can be seen from Fig. 4, the energy sparsity of the data may change with time and is affected by factors such as the environment and weather. In general, the sparsity stability of wavelet decomposition coefficients is better than DCT and FFT. The sparsity change of adjacent days does not exceed 4, and the sparsity of the whole analysis range does not exceed 10, but it can capture more than 99% of the data.

D. SPATIAL SIMILARITY

The previous sections have analyzed the sparseness and time stability of the MMD. This section analyzes the sparse mode between different sensors. Still based on several commonly used transformations described in Section IV.A, transform the data into sparse coefficients. The average and normalized sparse matrix $\boldsymbol{X}$ is plotted as shown in Fig. 5. Arranged according to different transformations, different columns in each block correspond to different sensing positions, and rows correspond to sparse coefficients.

As shown in Fig. 5, most of the coefficients are close to or equal to 0, and only a few top coefficients occupy most of the energy, which again reflects the sparsity of the data. More importantly, although the sensors are far apart (the latitude and longitude differ by a few degrees or even tens of degrees), the support set for each sensor is very similar, that is, the data have a spatial similarity. This is also determined by the nature of the sparse transform. For example, the energy of the DCT transform is concentrated in the low frequency part. The scale coefficients after the wavelet transform occupy most of the energy, which constitutes the priori about the support set.

Therefore, the problem of acquisition and reconstruction of MMD can be summarized as a joint reconstruction problem of multiple sparse signals with the same support set, just as described in Section III.A, satisfying the MMV model.

V. RECONSTRUCTION ALGORITHM AND ITS PERFORMANCE ANALYSIS

A. MINIMALIST RECONSTRUCTION ALGORITHM

Specific steps are described in Algorithm 1

In Algorithm 1, the sparse basis Ψ is selected according to Section IV.C, and the initial support set is preset to be the first K coefficients. As in the wavelet transform, these coefficients correspond to the scale coefficients occupying the main energy. The data are reconstructed using the a priori support set and the residual $\boldsymbol{R}^l$ is updated.

Algorithm 1 Minimalist Reconstruction (MR)

Input	Multiple observation vectors $\boldsymbol{Y}$, Measurement matrix Φ	
Output	t frame reconstruction data matrix $\hat{\boldsymbol{D}}$	
Step 1	Initialization	$\hat{\boldsymbol{X}}^0 = \boldsymbol{0}$, generate $\boldsymbol{\Psi}$ and estimate $K, \boldsymbol{A} = \Phi \cdot \Psi$, $l = 0, T^0 = \{1 : K\}$;
Step 2	Apriori Support Set Reconstruction	$\hat{\boldsymbol{X}}^l = \boldsymbol{A}_{T^0}^{\dagger}\boldsymbol{Y}, \boldsymbol{R}^l = \boldsymbol{Y} - \boldsymbol{A}\hat{\boldsymbol{X}}^l$;
Step 3	SMV Support Set Reconstruction	$l = l + 1$, $i = \text{randperm}\,(n, 1)$, $T^l = T^{l-1} \cup$ Sup-OMP $(\boldsymbol{A}, \boldsymbol{R}^l_{:,i})$;
Step 4	MMV Reconstruction	$\hat{\boldsymbol{X}}^l_{T^l} = \boldsymbol{A}^{\dagger}_{T^l}\boldsymbol{Y}$;
Step 5	Update	$\boldsymbol{R}^l = \boldsymbol{Y} - \boldsymbol{A}\hat{\boldsymbol{X}}^l$, IF $\left\|\boldsymbol{R}^l\right\|_F \geq \left\|\boldsymbol{R}^{l-1}\right\|_F$ output $\hat{\boldsymbol{D}} = \Psi\hat{\boldsymbol{X}}^{l-1}$, ELSE Go back to step 3.

Algorithm 2 Support Orthogonal Matching Pursuit (Sup-OMP)

Input	Observation vectors $\boldsymbol{y}$, Sensing matrix $\boldsymbol{A}$	
Output	Recovery support set Ω	
Step 1	Initialization	$\hat{\boldsymbol{x}}^0 = \boldsymbol{0}, \boldsymbol{r}^0 = \boldsymbol{y}, l = 0$, $T^0 = \emptyset$;
Step 2	Support set expansion	$l = l + 1$, $j = \arg\max_{i \notin T^{l-1}} \left\|\boldsymbol{A}_i^{\mathrm{T}}\boldsymbol{r}_{l-1}\right\|$, $T^l = T^{l-1} \cup \{j\}$;
Step 3	Reconstruction	$\hat{\boldsymbol{x}}^l = \arg\min_{\sup p(\boldsymbol{x}) \in T^l} \|\boldsymbol{A}\boldsymbol{x} - \boldsymbol{y}\|_2^2$;
Step 4	Update	$\boldsymbol{R}^l = \boldsymbol{Y} - \boldsymbol{A}\hat{\boldsymbol{X}}^l, \boldsymbol{r}^l = \boldsymbol{y} - \boldsymbol{A}\hat{\boldsymbol{x}}^l$, F $\left\|\boldsymbol{r}^l\right\|_2 \geq \left\|\boldsymbol{r}^{l-1}\right\|_2$ output $\Omega = T^{l-1}$, ELSE Go back to step 2.

rantperm(n,1) randomly generates an integer in [1,n] in order to randomly select one of the sensors for SMV support set reconstruction. The support set can be recovered using the OMP algorithm, referred to herein as Sup-OMP to distinguish, as shown in Algorithm 2. As analyzed in Section IV.D, the support set is the same under the MMV problem, so by randomly selecting a column, reducing the dimension to the SMV recovery support set can greatly reduce the amount of computation. Finally, the MMV problem is reconstructed with the restored support set. The residual is used to control the iterative process. If the residual is found to be expanded, the iteration is stopped and the last reconstruction result is output.

After random sparse sampling, the whole algorithm makes full use of the sparsity prior of MMD, and locks the key support set in advance (that is, the part that accounts for the majority of energy). Based on the spatial correlation dimension reduction data processing process, only a small amount of data are used to restore the support set, then reconstruct the entire MMV problem. The computation and traffic of the marine detection system are greatly reduced, so it is called the "minimalist" algorithm. The performance is analyzed below.

B. MEASUREMENT MATRIX RESTRICTED ISOMETRY PROPERTY

In this section, we first prove that the measurement matrix generated by distribution (3) satisfies the restricted isometry property (RIP). The main results will be based on the Geršgorin circle theorem and Hoeffding's inequality.

Definition 2 [26]: (RIP) if the matrix $\boldsymbol{\Phi}$ of $M \times N$ dimension satisfies

$$(1 - \delta_K)\|z\|_2^2 \leq \|\boldsymbol{\Phi}_T z\|_2^2 \leq (1 + \delta_K)\|z\|_2^2 \tag{7}$$

and holds for any vector $z \in \mathbb{R}^N$ with only K term non-zero coefficients. Then, the matrix $\boldsymbol{\Phi}$ is said to satisfy the K-order RIP with the parameter $\delta_K \in [0, 1)$, which is abbreviated as $\boldsymbol{\Phi} \in \text{RIP}\,(K, \delta_K)$.

In other words, if the eigenvalues of the Gram matrix corresponding to the sub-array composed of K columns in $\boldsymbol{\Phi}$ is in the range $[1 - \delta_K, 1 + \delta_K]$, then $\boldsymbol{\Phi}$ satisfies RIP (K, δ_K), so for a sparse vector that does not exceed K non-zero terms, $\boldsymbol{\Phi}$ is an isometry.

Lemma 1 (Geršgorin): The eigenvalues of an $N \times N$ matrix $\boldsymbol{\Phi}$ all lie in the union of N discs $d_i = d_i\,(c_i, r_i)$, $i = 1, 2, \cdots, N$ centered at $c_i = \phi_{i,i}$ and with radius

$$r_i = \sum_{\substack{j=1 \\ j \neq i}}^{N} \left|\phi_{i,j}\right| \tag{8}$$

where $\phi_{i,i}$ and $\phi_{i,j}$ are the diagonal elements and the non-diagonal elements of matrix $\boldsymbol{\Phi}$, respectively.

There are a total of C_N^K sub-matrices consisting of K columns extracted from the matrix $\boldsymbol{\Phi}$. If it is sequentially proved that the eigenvalues of each sub-matrix Gram matrix are respectively located at $[1 - \delta_K, 1 + \delta_K]$, then this will be a combinatorial complexity problem.

Therefore, we may consider an arbitrary column support set $T \subset \{1, \ldots, N\}$, $|T| \leq K$, and $\boldsymbol{\Phi}_T$ is a sub-matrix formed by columns indexed by T in $\boldsymbol{\Phi}$.

The Gram matrix of the matrix $\boldsymbol{\Phi}_T$ is $G\,(\boldsymbol{\Phi}_T) = \boldsymbol{\Phi}_T^{\mathrm{T}}\boldsymbol{\Phi}_T$. To prove that all the eigenvalues are in the range of $[1-\delta_k, 1+\delta_k]$, $\delta_d, \delta_o > 0$ can be appropriately selected to meet $\delta_d + K\delta_o = \delta_k \in (0, 1)$. If the diagonal elements g_{ii} of the $G\,(\boldsymbol{\Phi}_T)$ satisfy $|g_{ii} - 1| < \delta_d$, and the non-diagonal elements $g_{ij} (i \neq j)$ satisfy $\left|g_{ij} - 1\right| < \delta_o$, the distance between the center of each Geršgorin disk and 1 does not exceed δ_d, and the radius of each disk does not exceed $K\delta_o$. The range of values for

diagonal and non-diagonal elements can be determined by the following lemma

Lemma 2 (Diagonal Element Boundary): Considering $g_{i,i}$ as the diagonal element of the above-mentioned Gram matrix, $g_{ii} = \sum_{j=1}^{M} \phi_{ji}^2$, $i \in T$, and each element ϕ_{ji} is independent and identically distributed in (3), then

$$\Pr\left(|g_{ii} - 1| \geq \delta_d\right) \leq 2\exp\left(-2Mp\delta_d^2\right) \tag{9}$$

Proof: By Hoeffding's inequality [27], M independent bounded random variables $z_i \in [L_i, H_i]$according to probability 1, where only k elements are non-zero, maybe for the first k, and the sequence $s = \sum_{i=1}^{k} z_i$ satisfies

$$\Pr\left(|s - \mathbb{E}[s]| \geq \delta\right) \leq 2\exp\left[-\frac{2\delta^2}{\sum_{i=1}^{k}(H_i - L_i)^2}\right] \tag{10}$$

Let $z_i = \phi_{ji}^2$, from the distribution of the formula (3), $z_i \in \left[0, 1/(Mp)\right]$ is established according to the probability 1. Considering that only $k = Mp$ elements of the M summation terms are non-zero according to the distribution, $s = g_{ii}$, $\mathbb{E}[g_{ii}] = M\mathbb{E}\left[\phi_{ji}^2\right] = 1$, substituting into (10)

$$\Pr\left(|g_{ii} - \mathbb{E}[g_{ii}]| \geq \delta_d\right) \leq 2\exp\left(-\frac{2\delta_d^2}{Mp\left(1/M^2p^2\right)}\right) \tag{11}$$

Thus, (9) is proved.

Lemma 3 (Non-Diagonal Element Boundary): g_{ij} is the diagonal element of the above-mentioned Gram matrix, $g_{ij} = \sum_{r=1}^{M} \phi_{ri} \cdot \phi_{rj}$, $i, j \in T$, and each element is independently and identically distributed in the formula (3), then

$$\Pr\left\{\left|g_{ij}\right| \geq \delta_o\right\} \leq 2\exp\left[-\frac{M\delta_o^2}{2}\right] \tag{12}$$

Proof: still using Hoeffding's inequality (10), at this time, $z_i = \phi_{ri}\phi_{rj}$, $z_i \in \left[-1/(Mp), 1/(Mp)\right]$, $s = \sum_{i=1}^{M} z_i = g_{ij}$, $\mathbb{E}[s] = 0$. Notice that there are only $k = Mp^2$ of M elements non-zero according to the distribution. Substitute into (10), then

$$\Pr\left(\left|g_{ij}\right| \geq \delta_o\right) \leq 2\exp\left[-\frac{2\delta^2}{Mp^2\left(2/Mp\right)^2}\right] \tag{13}$$

Formula (12) is proved.

Theorem 1: $\boldsymbol{\Phi}$ is an $M \times N$ dimensional random matrix, and each element is i.i.d in the distribution of formula (3). Then, for any $\varepsilon, \delta_K \in (0, 1)$, when the sampling rate $r = Mp \geq \frac{2\ln 2K^2}{c^2\delta_K^2 - \varepsilon}$, $\boldsymbol{\Phi}$ satisfies the K-order RIP with a probability of not less than $1 - \exp\left[-Mp\varepsilon/2\right]$.

Proof: arbitrary column support set $T \subset \{1, \ldots, N\}$, $|T| = K$, $\boldsymbol{\Phi}_T$ is a submatrix composed of columns indexed by Tin $\boldsymbol{\Phi}$, and its corresponding Gram matrix is$G(\boldsymbol{\Phi}_T) = \boldsymbol{\Phi}_T^{\mathrm{T}}\boldsymbol{\Phi}_T$. By Lemma 2, for all g_{ii} satisfied

$$\Pr\left(\bigcup_{i=1}^{K}|g_{ii} - 1| \geq \delta_d\right) \leq 2K\exp\left(-2Mp\delta_d^2\right) \tag{14}$$

At the same time, consider that the non-diagonal elements of $G(\boldsymbol{\Phi}_T)$ have symmetry, and there are a total of $K(K-1)/2$ non-diagonal elements that are different from each other. By Lemma 3, all g_{ij} joint probability distributions satisfy.

$$\Pr\left\{\bigcup_{i=1}^{K}\bigcup_{\substack{j=1\\ j\neq i}}^{K}\left|g_{ij}\right| \geq \delta_o\right\} \leq K^2\exp\left[-\frac{M\delta_o^2}{2}\right] \tag{15}$$

According to Lemma 1, the probability that all the eigenvalues of $G(\boldsymbol{\Phi}_T)$ are located in the disc (within $[1 - \delta_K, 1 + \delta_K]$) is P, which is known from (14) and (15).

$$\begin{aligned}\bar{P} &= \Pr\left(\bigcup_{i=1}^{K}[|g_{ii} - 1| \geq \delta_d]\right) + \Pr\left\{\bigcup_{i=1}^{K}\bigcup_{\substack{j=1\\ j\neq i}}^{K}\left|g_{ij}\right| \geq \delta_o\right\} \\ &\leq 2K\exp\left(-2Mp\delta_d^2\right) + K^2\exp\left[-\frac{M\delta_o^2}{2}\right]\end{aligned}$$

Because $\delta_d + K\delta_o = \delta_k$, and $\delta_o = c\delta_K$, $\delta_d = (1 - cK)\delta_K$, where $c \in \left(0, 1/K\right)$. Therefore,

$$\begin{aligned}&2K\exp\left(-2Mp\delta_d^2\right) + K^2\exp\left[-\frac{M\delta_o^2}{2}\right] \\ &\quad = 2K\exp\left[-2Mp\left(1 - cK\right)^2\delta_K^2\right] + K^2\exp\left[-\frac{Mc^2\delta_K^2}{2}\right]\end{aligned}$$

Take $c \in \left(0, \frac{1}{K}\right) \setminus \left[\frac{2}{2K+1}, \frac{2}{2K-1}\right]$, then $2\left(1 - cK\right)^2 > \frac{c^2}{2}$, so

$$\bar{P} \leq 2K^2\exp\left[-\frac{Mpc^2\delta_K^2}{2}\right] \tag{16}$$

For any $\varepsilon < c^2\delta_K^2$, when $Mp \geq \frac{2\ln 2K^2}{c^2\delta_K^2 - \varepsilon}$,

$$P > 1 - \exp\left[-\frac{Mp\varepsilon}{2}\right] \tag{17}$$

Since the column support set T, $|T| = K$ is arbitrarily selected, it has been proved that the probability that all the eigenvalues of the Gram matrix $G(\boldsymbol{\Phi}_T)$ are in the range of $[1 - \delta_K, 1 + \delta_K]$ is P. That is, the probability is P that the eigenvalues of all Gram matrix corresponding to the sub-matrix composed of no more than K columns in $\boldsymbol{\Phi}$ are in $[1 - \delta_K, 1 + \delta_K]$, which just satisfies the definition of RIP, and the theorem is proved.

In particular, when the orthogonal transform $\boldsymbol{\Psi}$ is employed, it is known from the norm-preserving properties of the orthogonal transform that the sensing matrix $\boldsymbol{A} = \boldsymbol{\Phi}\boldsymbol{\Psi}$ is also satisfied if $\boldsymbol{\Phi}$ meets the RIP.

C. RECONSTRUCTION GUARANTEE

Wen *et al.* [28] gave the sharp recovery conditions for the OMP algorithm under the SMV model, and Yang *et al.* [29] extended the conclusions of the SMV given by Mo and Shen [30] earlier to MMV. In the same way, we can also promote the sharp conditions under SMV.

Theorem 2: For a K rows sparse matrix $\boldsymbol{X}$, if the sensing matrix $\boldsymbol{A}$ satisfies RIP and

$$\delta_{K+1} < \frac{1}{\sqrt{K+1}} \tag{18}$$

the OMP algorithm can accurately recover the original data $\boldsymbol{X}$ from the MMV observation $\boldsymbol{Y} = \boldsymbol{AX}$. Proof can be found in references [28] and Theorem 3.5 in [29].

It can be seen from the description of Section V.A algorithm that the minimalist algorithm is an OMP recovery with a known support set of prior conditions. Therefore, δ_K is determined according to the theorem 2 for the sparsity K, and then the sampling scale Mp is determined by theorem 1, and finally control the probability P of the exact reconstruction. The following uses the measured data to investigate the overall performance of the CS-MMD scheme with the space-time sampling and minimalist reconstruction proposed in this paper.

VI. PERFORMANCE EVALUATION

The overall performance of the CS-MMD scheme was evaluated using the TAO measured data mentioned in Section IV.

A. RECONSTRUCTION ACCURACY ANALYSIS

As described in Section III.B, the sampling size is controlled by adjusting the number of rows M and the probability p of the non-zero elements in the measurement matrix. According to the analysis of IV.A and IV.C, the sparseness of the wavelet decomposition coefficients of MMD is better than DCT and FFT. The Haar decomposition coefficients energy sparsity K is the smallest about 2, and K of the Sym4 coefficients is the largest about 8. Therefore, this section uses these two wavelet bases as an example to analyze the compressed sensing sampling and reconstruction of four typical MMD (AirT, Rhum, SST and WS). Analyzing the relative error (RE) of the reconstructed data compared to the original data, defined as

$$\mathrm{RE} = \frac{\left\|\hat{\boldsymbol{D}} - \boldsymbol{D}\right\|_{\mathrm{F}}^2}{\|\boldsymbol{D}\|_{\mathrm{F}}^2} \tag{19}$$

Its physical meaning is the ratio of the data energy lost by the compressed sensing reconstruction process to the original data energy.

Fig.6 and Fig.7 show the case where the RE of the CS-MMD scheme changes with M and p when the sparse basis selects the Haar and Sym4 wavelets respectively, and the value is described in gray scale. From the trend in the figures, RE decreases with the increase of M and p. As described in Section III.B, the ratio of the sample number in this method to it in the traditional method is $r = Mp$. The more the number of samples, the higher the reconstruction accuracy, and the theorem 1 is verified.

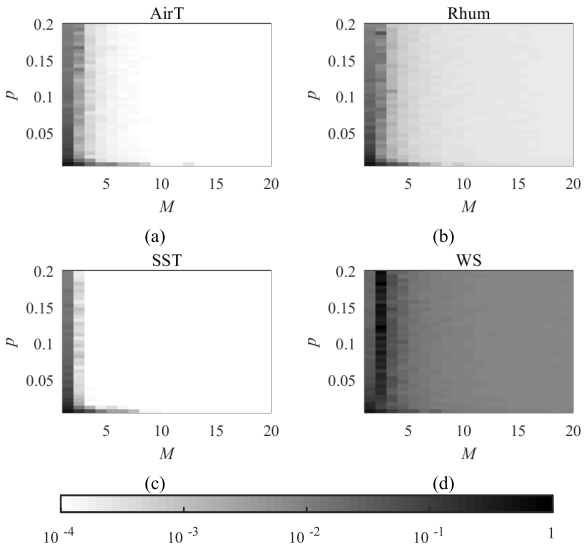

FIGURE 6. RE v.s. p & M (Haar).

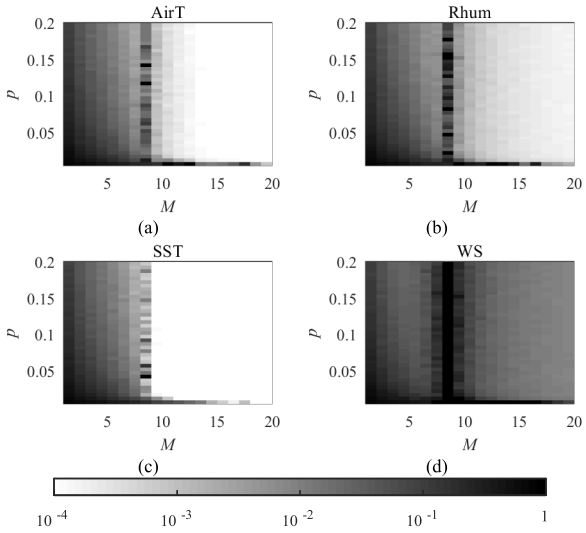

FIGURE 7. RE v.s. p & M (Sym4).

It can be seen from Fig.6 that the relative errors of AirT, Rhum and SST converge to 10^{-4} orders of magnitude, and the error of WS converges to 10^{-2} orders, which is in accordance with the analysis in Sections IV.A and IV.C. Because for the Haar wavelet base, the scale coefficients will capture 99.98%, 99.9%, 99.93%, and 92.6% of the energy of AirT, Rhum, SST, and WS, respectively, indicating that CS-MMD accurately restores at least significant scale coefficients and recovers partial wavelet coefficients.

Comparing Fig.6 and Fig.7, it is found that the same data have different requirements for M, because for Haar wavelet base, K is about 2, and under Sym4, K is about 8. It can be seen from Fig.7 that the observation number should be at least greater than K to ensure the reconstruction accuracy of the data. The convergence error is in accordance with the

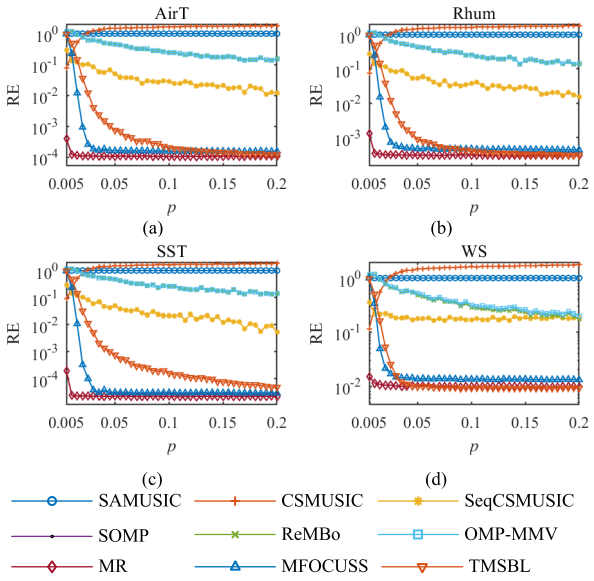

FIGURE 8. RE v.s. p (Haar).

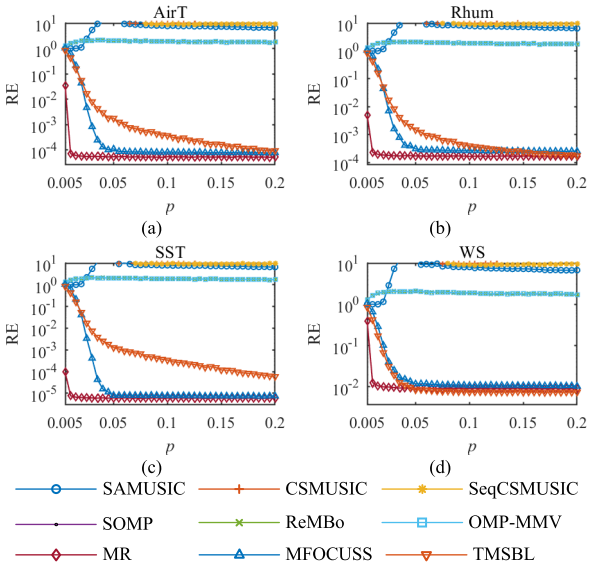

FIGURE 9. RE v.s. p (Sym4).

analysis in Sections IV.A and IV.C, because for the Sym4 wavelet base, the scale coefficients will capture 99.99%, 99.96%, 99.98%, and 96.48% of the energy of AirT, Rhum, SST and WS respectively.

The following analyzes the reconstruction performance of similar algorithms.

B. THE RELATIONSHIP BETWEEN RECONSTRUCTION ERROR AND PROBABILITY P OF DIFFERENT ALGORITHMS

In Section II, the commonly used recovery algorithms include greedy algorithms, minimization optimization algorithms and Bayesian algorithms. Here, several representative algorithms in each class are selected as controls. The number of observations M is fixed at $2K$, the probability is increased from 0.005 to 0.2 in steps of 0.005, and the probability of reconstruction relative error with the probability p of non-zero elements in the measurement matrix is shown in Fig.8. The sparse basis $\mathbf{\Psi}$ is the Haar wavelet basis. From the results, the reconstruction errors of TMSBL, MFOCUSS and MR proposed in this paper are all converge, and the relative errors of AirT, Rhum and SST converge to the order of 10^{-4}. The error of WS converges to the order of 10^{-2} consistent with the analysis in Sections IV.A, IV.C, and VI.A.

From the results of Fig.8, it is shown that TMSBL, MFOCUSS and MR can accurately recover the scale coefficients occupied most energy and recover part of the wavelet coefficients with a small amount of observation data. In particular, it is noted that the CS-MMD scheme proposed in this paper can be converged first under the severe conditions of $p = 0.01$. It is known from the physical meaning of p that it describes the working probability of the original sensor, in other words, the premise of saving 99% of sampling resources. The accuracy rate can be as high as 99% or more. Parameters like WS, although the sparsity is slightly weaker, can achieve an accuracy of 92.6%.

The performance of other algorithms in the control group is not ideal. The performances of the three improved OMP algorithms are similar because they do not use the support set prior. Once an iteration has selected wrong atoms, subsequent iterations will be difficult to recover the error that has already occurred due to the lack of a culling mechanism. Among the three improved MUSIC algorithms, SeqCSMUSIC performs relatively well, but it is not ideal enough. The problem is that such methods are mainly oriented to solving the sparse reconstruction problem in the ℓ_0 norm sense, and some require sparsity to be known. However, the MMD here are not sparse in the ℓ_0 norm, so the performance of the algorithm is limited.

In order to compare the effect of energy sparsity on performance, next, the sparse basis selects the Sym4 wavelet base. From IV.C analysis, the energy sparsity K is about 8. At this time, the relative errors of the reconstructed energy of the four kinds of data change with p as shown in Fig.9. The reconstruction errors of TMSBL, MFOCUSS and the MR proposed in this paper are all converge to the level analyzed in Sections IV.A, IV.C, and VI.A. When the above three algorithms converge, at least the scale coefficients are accurately restored, and some wavelet coefficients are restored. The requirements of p for convergence of each algorithm have increased. It is noted that the CS-MMD scheme proposed in this paper can still be converged under severe conditions of $p = 0.01$.

The three improved OMP algorithms and the three MUSIC improved algorithms in the control group basically failed. This is because when the energy sparsity increases, the energy of each coefficient is relatively dispersed. When the data sparsity in the sense of ℓ_0 norm does not exist and the sparsity is unknown, the reconstruction support sets by the above two types of algorithms are prone to ambiguity, especially when the number of observations is relatively small.

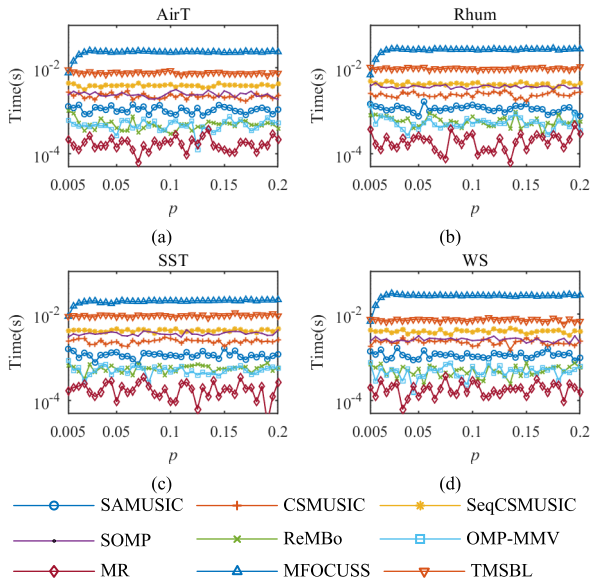

FIGURE 10. Time v.s. p (Haar).

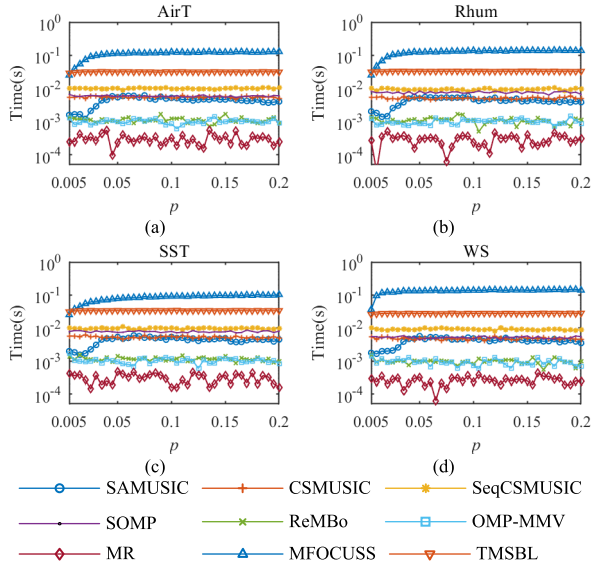

FIGURE 11. Time v.s. p (Sym4).

C. RELATIONSHIP BETWEEN RECONSTRUCTION TIME AND SAMPLING RATE

Next, we will examine the trend of the running time of each algorithm with p. Fig.10 shows results under the Haar wavelet base. The operation results under the Sym4 wavelet base are shown in Fig.11. The overall trend conforms to the general law, that is, the minimization optimization algorithm has higher complexity, the greedy algorithm is simpler, and the Bayesian algorithm complexity is between the two. Although the CS-MMD scheme of this paper is also extended on the basis of OMP, it makes full use of the support set priori compared with ReMBo and OMP-MMV, which greatly reduces the number of iterations. So, the calculation time of CS-MMD is the shortest, and the average is within 10^{-4} second order. Compared with the other two algorithms, MFOCUSS and TMSBL with better performance in Section VI.B, the time complexity of our scheme is reduced by more than two orders of magnitude.

The energy sparsity increases under the Sym4 wavelet base, so the number of iterations may increase, thus the running time of each algorithm generally increases. However, the CS-MMD scheme in this paper is not affected by the increase of energy sparsity, and the time complexity is still maintained at 10^{-4} order, because most of the iteration has been omitted by the prior support set. Therefore, through the analysis of this part, the idea of "simple and simple" in our paper are verified, that is, reducing the number of samples and simplifying the reconstruction by dimension reduction. Our scheme fully adapts to the situation where the energy and traffic of the maritime monitoring system are limited.

VII. CONCLUSION

This paper proposes a CS-MMD scheme that uses the simplest possible solution that can be taken to get the best results that can be achieved. A highly sparse random matrix is used to collect a small number of measurements. Based on the natural energy sparsity characteristics of the data, the wavelet base is selected, and the a priori support set generated by the significant wavelet coefficients is fully utilized. Meanwhile, the MMV problem is randomly reduced into SMV for reconstruction. Considering that the power and communication capacity of the marine data acquisition system are limited, each step saves resources, simplifies the process, and makes full use of the sparse features of the data, and finally accurately and efficiently reconstructs the data. Accuracy can reach 99% or more on the premise of saving 99% of sampling resources.

Of course, the sparse basis is the key to determine the energy sparsity of the data, and then determines the performance of the reconstruction. This paper considers the overall complexity of the system, therefore, the off-the-shelf DCT, FFT and several wavelet bases are selected for comparison. Other sparse dictionaries that require a complex dictionary learning process are not considered. This will be a key point in the follow-up study, which is to discuss a dictionary with low complexity and good energy concentration. This is another topic.

ACKNOWLEDGMENT

Thanks to the GTMBA Project Office of NOAA/PMEL for providing TAO project data.

REFERENCES

[1] Y. Shi, Q. Zhang, S. Wang, K. Yang, Y. Yang, X. Yan, and Y. Ma, "A comprehensive study on maximum wavelength of electromagnetic propagation in different evaporation ducts," *IEEE Access*, vol. 7, pp. 82308–82319, 2019.

[2] X. Zhu, J. Li, M. Zhu, Z. Jiang, and Y. Li, "An evaporation duct height prediction method based on deep learning," *IEEE Geosci. Remote Sens. Lett.*, vol. 15, no. 9, pp. 1307–1311, Sep. 2018.

[3] X. Yan, K. Yang, and Y. Ma, "Calculation method for evaporation duct profiles based on artificial neural network," *IEEE Antennas Wireless Propag. Lett.*, vol. 17, no. 12, pp. 2274–2278, Dec. 2018.

[4] J. Pozderac, J. Johnson, C. Yardim, C. Merrill, T. de Paolo, E. Terrill, F. Ryan, and P. Frederickson, "*X*-band beacon-receiver array evaporation duct height estimation," *IEEE Trans. Antennas Propag.*, vol. 66, no. 5, pp. 2545–2556, May 2018.
[5] K. Xie, L. Wang, X. Wang, G. Xie, and J. Wen, "Low cost and high accuracy data gathering in WSNs with matrix completion," *IEEE Trans. Mobile Comput.*, vol. 17, no. 7, pp. 1595–1608, Jul. 2018.
[6] F. Fazela, M. Fazelb, and M. Stojanovica, "Compressed sensing in random access networks with applications to underwater monitoring," *Phys. Commun.*, vol. 5, no. 2, pp. 148–160, 2012.
[7] S. Zhuang, W. Zhao, R. Wang, Q. Wang, and S. Huang, "New measurement algorithm for supraharmonics based on multiple measurement vectors model and orthogonal matching pursuit," *IEEE Trans. Instrum. Meas.*, vol. 68, no. 6, pp. 1671–1679, Jun. 2019.
[8] M. Yuan and W. Zhong, "Detecting intensity evolution of the western north pacific super typhoons in 2016 using the deviation angle variance technique with FY data," *J. Meteorolog. Res.*, vol. 33, no. 1, pp. 104–114, Feb. 2019.
[9] J. W. Choi and B. Shim, "Statistical recovery of simultaneously sparse time-varying signals from multiple measurement vectors," *IEEE Trans. Signal Process.*, vol. 63, no. 22, pp. 6136–6148, Nov. 2015.
[10] Y. Jin and B. D. Rao, "Support recovery of sparse signals in the presence of multiple measurement Vectors," *IEEE Trans. Inf. Theory*, vol. 59, no. 5, pp. 3139–3157, May 2013.
[11] J. Zou, Y. Fu, Q. Zhang, and H. Li, "Split Bregman algorithms for multiple measurement vector problem," *Multidimensional Syst. Signal Process.*, vol. 26, no. 1, pp. 207–224, Jan. 2015.
[12] S. F. Cotter, B. D. Rao, K. Engan, and K. Kreutz-Delgado, "Sparse solutions to linear inverse problems with multiple measurement vectors," *IEEE Trans. Signal Process.*, vol. 53, no. 7, pp. 2477–2488, Jul. 2005.
[13] S. Khanna and C. R. Murthy, "Sparse recovery from multiple measurement vectors using exponentiated gradient updates," *IEEE Signal Process. Lett.*, vol. 25, no. 10, pp. 1485–1489, Oct. 2018.
[14] Z. Chen, R. Molina, and A. K. Katsaggelos, "Robust recovery of temporally smooth signals from under-determined multiple measurements," *IEEE Trans. Signal Process.*, vol. 63, no. 7, pp. 1779–1791, Apr. 2015.
[15] S. Narayanan, S. K. Sahoo, and A. Makur, "Greedy Pursuits Assisted Basis Pursuit for reconstruction of joint-sparse signals," *Signal Process.*, vol. 142, no. 1, pp. 485–491, Jan. 2018.
[16] J. D. Blanchard, M. Cermak, D. Hanle, and Y. Jing, "Greedy algorithms for joint sparse recovery," *IEEE Trans. Signal Process.*, vol. 62, no. 7, pp. 1694–1704, Apr. 2014.
[17] K. Lee, Y. Bresler, and M. Junge, "Subspace methods for joint sparse recovery," *IEEE Trans. Inf. Theory*, vol. 58, no. 6, pp. 3613–3641, Jun. 2012.
[18] J. M. Kim, O. K. Lee, and J. C. Ye, "Compressive MUSIC: Revisiting the link between compressive sensing and array signal processing," *IEEE Trans. Inf. Theory*, vol. 58, no. 1, pp. 278–301, Jan. 2012.
[19] M. E. Davies and Y. C. Eldar, "Rank awareness in joint sparse recovery," *IEEE Trans. Inf. Theory*, vol. 58, no. 2, pp. 1135–1146, Feb. 2012.
[20] J. D. Blanchard and M. E. Davies, "Recovery guarantees for rank aware pursuits," *IEEE Signal Process. Lett.*, vol. 19, no. 7, pp. 427–430, Jul. 2012.
[21] Z. Zhang and B. D. Rao, "Sparse signal recovery with temporally correlated source vectors using sparse Bayesian learning," *IEEE J. Sel. Topics Signal Process.*, vol. 5, no. 5, pp. 912–926, Sep. 2011.
[22] M. Ghadyani and A. Shahzadi, "Compressive Sampling Rate Optimization for Multiple Measurement Vector Problems," *Iranian J. Sci. Technol., Trans. Electr. Eng.*, vol. 43, no. S1, pp. 101–108, Jul. 2019.
[23] L. Li, X. Huang, and J. A. K. Suykens, "Signal recovery for jointly sparse vectors with different sensing matrices," *Signal Process.*, vol. 108, pp. 451–458, Mar. 2015.
[24] K. G. Deepa, S. K. Ambat, and K. V. S. Hari, "Fusion of Sparse Reconstruction Algorithms for Multiple Measurement Vectors," *Sādhanā*, vol. 41, no. 11, pp. 1275–1287, Nov. 2016.
[25] E. J. Candès and T. Tao, "Near-optimal signal recovery from random projections: Universal encoding strategies?" *IEEE Trans. Inf. Theory*, vol. 52, no. 12, pp. 5406–5425, Dec. 2006.
[26] E. J. Candès, "The restricted isometry property and its implications for compressed sensing," *Comp. Rendus Math.*, vol. 346, nos. 9–10, pp. 589–592, May 2008.
[27] J. Haupt, W. U. Bajwa, G. Raz, and R. Nowak, "Toeplitz compressed sensing matrices with applications to sparse channel estimation," *IEEE Trans. Inf. Theory*, vol. 56, no. 11, pp. 5862–5875, Nov. 2010.
[28] J. Wen, Z. Zhou, J. Wang, X. Tang, and Q. Mo, "A sharp condition for exact support recovery with orthogonal matching pursuit," *IEEE Trans. Signal Process.*, vol. 65, no. 6, pp. 1370–1382, Mar. 2017.
[29] X. Yang, A. Liao, and J. Xie, "A remark on joint sparse recovery with OMP algorithm under restricted isometry property," *Appl. Math. Comput.*, vol. 316, no. 1, pp. 18–24, Jan. 2018.
[30] Q. Mo and Y. Shen, "A remark on the restricted isometry property in orthogonal matching pursuit," *IEEE Trans. Inf. Theory*, vol. 58, no. 6, pp. 3654–3656, Jun. 2012.

WENBIAO TIAN was born in Nanchang, China, in 1987. He received the B.Sc., M.Sc., and Ph.D. degrees in information and communication engineering from Naval Aeronautical and Astronautical University, Yantai, China, in 2008, 2010, and 2014, respectively.

Since 2018, he has been an Associate Professor with the Signal and Information Processing Provincial Key Laboratory in Shandong, Naval Aviation University, Yantai. His research interests include signal processing, sparse and low-rank problems, and statistical approaches to inverse problems.

GUOSHENG RUI was born in Nanjing, China, in 1968. He received the B.S. degrees in radio technology from the Hefei University of Technology, Hefei, China, in 1990, the M.S. degree in communication and electronics from Naval Aeronautical and Astronautical University, Yantai, China, in 1995, and the Ph.D. degree in signal and information processing from the Harbin Institute of Technology, Harbin, China, in 2001.

From 1995 to 2001, he was a Lecturer with the Department of Electronics and Information Engineering, Naval Aviation University. From 2002 to 2006, he was an Associate Professor. Since 2007, he has been a Professor with the Signal and Information Processing Provincial Key Laboratory in Shandong, Naval Aviation University, Yantai. He has published extensively in the areas of weak signal processing and communications (over 200 journal articles, 50 conference papers, and three books), and he holds 25 patents. He has supervised ten Ph.D. theses. His research interests include weak signal processing, sparse and low-rank problems, and Bayesian modeling and inference.

GE LIU was born in Weihai, Shandong, in 1991. She received the B.S. degree, in 2014, and the M.S. degree, in 2016. She is currently pursuing the Ph.D. degree in information and communication engineering with Navy Aviation University. Her main research interest includes dynamic compressive sensing.

DAOGUANG DONG was born in Jinan, Shandong, in 1990. He received the B.S. degree, in 2013, and the M.S. degree, in 2015. He is currently pursuing the Ph.D. degree in information and communication engineering with Navy Aviation University. His main research interests include Bayesian statistical learning and compressed sensing.